[(C^C)Au(N^N)]+ complexes as a new family of anticancer candidates: synthesis, characterization and exploration of the antiproliferative properties

Silva Khodjoyan,[a] Edwyn Remadna,[a] Héloïse Dossmann,[a] Denis Lesage,[a] Geoffrey Gontard,[a] Jérémy Forté,[a] Henrik Hoffmeister,[b] Uttara Basu,[b] Ingo Ott,[b] Philip Spence,[c] Zoë A. E. Waller,[c,d] Michèle Salmain[a] and Benoît Bertrand[a]*

[a] Sorbonne Université, CNRS, Institut Parisien de Chimie Moléculaire, IPCM, F-75005 Paris, France
[b] Institute of Medicinal and Pharmaceutical Chemistry, Technische Universität Braunschweig, Beethovenstrasse 55, D-38106 Braunschweig, Germany
[c] School of Pharmacy, University of East Anglia, Norwich, NR4 7TJ, United Kingdom
[d] UCL School of Pharmacy, 29-39 Brunswick Square, London WC1N 1AX, United Kingdom
Corresponding author e-mail: benoit.bertrand@sorbonne-universite.fr

Abstract

A library of eleven cationic gold(III) complexes of the general formula $[(C^C)Au(N^N)]^+$ when C^C is either biphenyl or 4,4'-ditertbutyldiphenyl and N^N is a bipyridine, phenanthroline or dipyridylamine derivative have been synthesized and characterized. Contrasting effects on the viability of the triple negative breast cancer cells MDA-MB-231 was observed from a preliminary screening. The antiproliferative activity of the seven most active complexes were further assayed on a larger panel of human cancer cells as well as on non-cancerous cells for comparison. Two complexes stood out for being either highly active or highly selective. Eventually, reactivity studies with biologically meaningful amino acids, glutathione, higher order DNA structures and thioredoxin reductase (TrxR) revealed a markedly different behavior from that of the well-known coordinatively isomeric $[(C^N^C)Au(NHC)]^+$ structure. This makes the $[(C^C)Au(N^N)]^+$ complexes a new class of organogold compounds with an original mode of action.

Introduction

In the last few decades, gold-based compounds have attracted particular attention as potential anticancer agents.[1,2] Although the mechanism of action of gold-based compounds has not been yet fully determined, it is widely accepted that their cytotoxic effect comes from the interaction and inhibition of enzymes[3] while the mechanism of action of platinum-based compounds mostly involves binding to DNA.[4] Among all gold-based compounds tested, gold(III) complexes have attracted particular interest as Au(III) is isoelectronic to Pt(II).[5] However, while the +II oxidation state of platinum is very stable in biological environment, the +III oxidation state of gold is generally not. However, this lack of stability can be overcome by using appropriate ligands which can improve the overall stability of the complex. In this manner, a large panel of ligands have been investigated for this purpose, to stabilize Au(III), and their antiproliferative properties have been tested against various cancer cell lines. The main classes of ligands explored to date are chelating N-donor ligands,[6,7]

porphyrins,[8] dithiocarbamates[9,10] as well as (C^N),[11,12] (C^N^N),[13] (C^N^C)[14,15] and very recently (C^N^N^C)[16] cyclometalated ligands as depicted in figure 1.

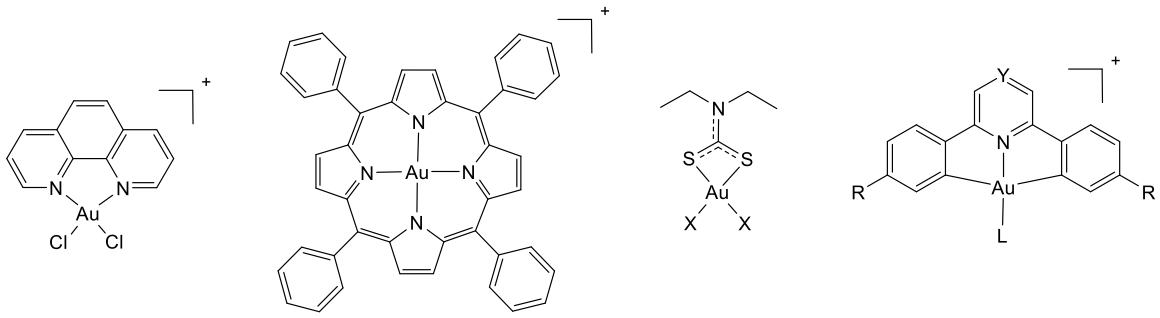

Figure 1: Examples of Au(III) complex families investigated for their antiproliferative properties.

Still, the main challenge in Au(III) medicinal chemistry is arguably the stabilization of the +III oxidation state. To this respect, $[(C^N^C)Au(NHC)]^+$ complexes have appeared especially promising, being stable even in the presence of the biological reductant glutathione (GSH).[15] In return, this high stability results in a lack of reactivity. Indeed, this class of compound is thought to trigger antiproliferative effects by interaction of the whole $[(C^N^C)Au(NHC)]^+$ entity with biological targets through π-stacking or electrostatic interactions.[15,17] This implies also a narrow spectrum of optimization possibly rendering the enhancement of the biological properties of this family of compounds quite difficult.[18,19] Considering that the high redox stability of $[(C^N^C)Au(L)]^+$ complexes mostly arises from the two Au-C_{Ph} bonds, they should be retained when designing new scaffolds. However, having the pyridine ring in between the two Au-C_{Ph} bonds prevents ligand de-coordination and thus decreases potential interactions with biological targets. This feature is even more pronounced in the case of $[(C^N^N^C)Au]^+$ scaffolds for which all the four coordination sites are blocked.[16] Thus, based on these statements, one way to improve the biological properties of $[(C^N^C)Au(L)]^+$ complexes would be to reorganize the coordination sphere around the Au(III) cation to preserve its redox stability while enhancing its reactivity.

With such an objective in mind, the use of biphenyl ligands (C^C) seemed of great potential since it would preserve the two Au-C_{Ph} bonds ensuring the redox stability while the remaining two coordination sites are available for binding other ligands. [(C^C)Au] complexes have been known since the early 80's[20] but have not been studied until the last decade, mostly for their photophysical properties[21,22] and as tools for reactivity investigations.[23,24] We have accordingly synthesized and characterized a library of cationic organogold(III) complexes bearing a stable (C^C) biphenyl ligand and a more labile (N^N) ligand analogous to the $[(C^N^C)Au(L)]^+$ and $[(C^N^N^C)Au]^+$ families as presented in figure 2. These eleven new $[(C^C)Au(N^N)]^+$ organogold complexes were obtained by variating the substituents on the biphenyl chelate and by using various classes of (N^N) ligands including bipyridine-, phenanthroline- and dipyridylamine-type ligands. Their antiproliferative properties were carefully determined on a range of human cancer cells derived from different organs/tissues (MDA-MB-231, MCF-7 and A2780) and a healthy cell line (MCF-10A) for comparison. The reactivity of the most interesting complexes with selected amino acids and GSH (reduced glutathione) was investigated by mass spectrometry revealing a very different reactivity compared to a $[(C^N^C)Au(NHC)]^+$ making $[(C^C)Au(N^N)]^+$ complexes a new class of gold-based anticancer candidates.

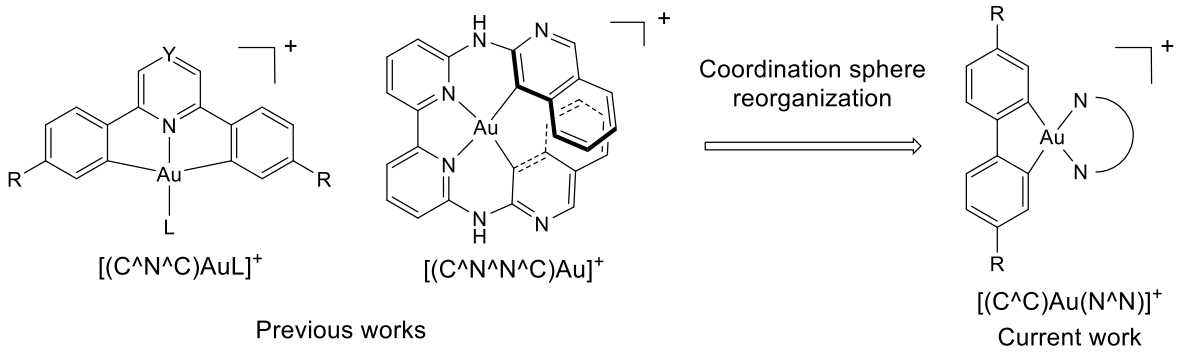

Figure 2: Comparison between the analogous $[(C^N^C)Au(L)]^+$, $[(C^N^N^C)Au]^+$ and $[(C^C)Au(N^N)]^+$ families.

Results and discussion

Synthesis

Eleven $[(C^C)Au(N^N)]^+$ complexes were synthesized by reaction of two different biphenyl Au(III) chloride dimer precursors carrying or not t-butyl groups with a range of N-donor ligands being either based on bipyridine, phenanthroline or 2,2'-dipyridylamine scaffolds followed by replacement of the chloride counterion by tetrafluoroborate using the corresponding silver salt according to a reported procedure (figure 3).[20] T-butyl groups were chosen to limit the aggregation of the formed complexes and thus enhance their solubity.

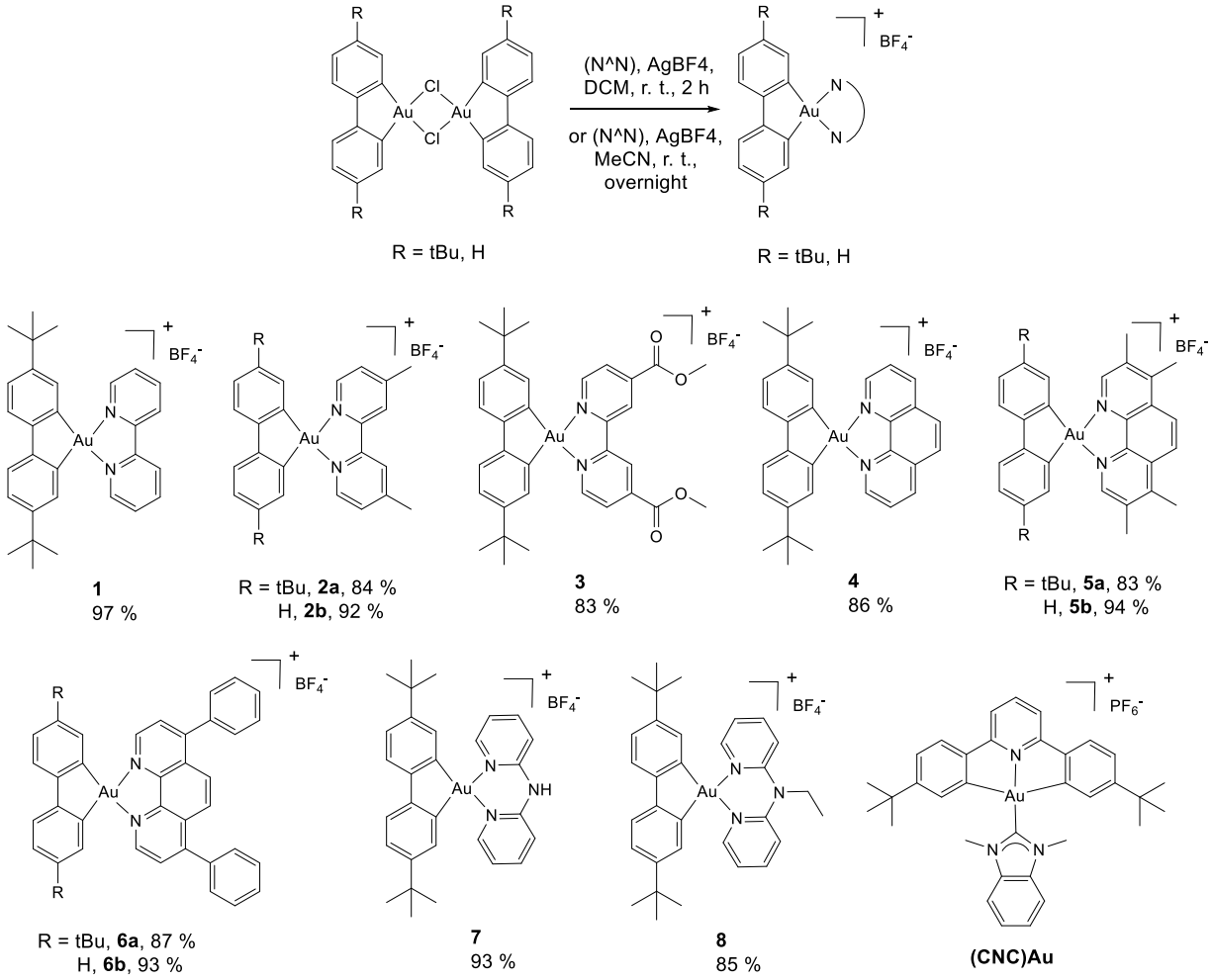

Figure 3: Synthesis and structure of [(C^C)Au(N^N^)]BF_4 complexes **1-8** and **(CNC)Au**.

Synthetic yields were higher than 80%, regardless of the (N^N) ligand leading to complexes **1** – **8**. The longer reaction time required for the biphenyl compounds (R = H, compounds **2b**, **5b** and **6b**) is due to the lower solubility of the dimeric precursor slowing down the reaction. Moreover, the synthetic procedure also appeared very tolerant to the nature of the substituents on the (N^N) ligand as demonstrated in the bipyridine series (compounds **1**-**3**). The structure of the $[(C^C)Au(N^N)]^+$ complexes was assessed by ^{1}H NMR spectroscopy, showing both the (C^C) and (N^N) chelates as symmetrical and in a 1/1 ratio. Interestingly while compounds **2a-b**, **4**, **5a-b**, **6a** and **8** gave ^{1}H NMR spectra with thin well-defined peaks, compounds **1**, **3**, **6b** and **7** gave ^{1}H NMR spectra with very broad peaks. The structure of $[(C^C)Au(N^N)]^+$ complexes was confirmed by HR-MS and their purity assessed by elemental analysis.

Solid state structures

Single crystals suitable for X-Ray diffraction (XRD) analysis of complexes **1**, **2a**, **3**, **5a** and **7** were grown by slow evaporation of a saturated solution of the compounds in a dichloromethane/toluene mixture at 4 °C. Crystal structures are depicted in figures 4 to 6 and S1-2. Main bond lengths are shown in table S1.

Note: Atoms numbering could be different between illustration of crystal structures and their CIF file available in CSD database.

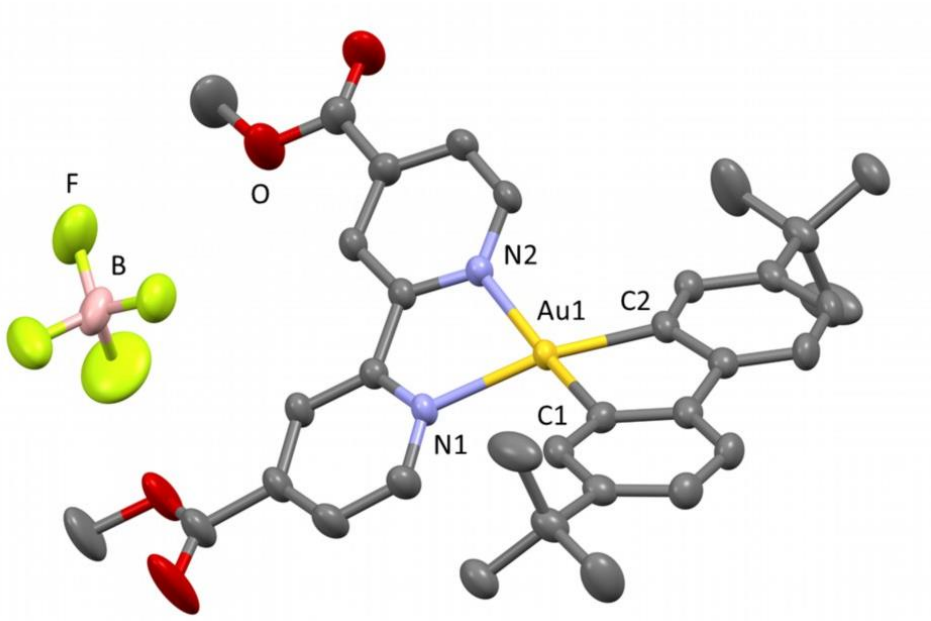

Figure 4: Crystal structure of complex **3**. Ellipsoids set at 50% probability. Hydrogen atoms and toluene have been omitted for clarity. Selected bond distances [Å] and angles [°] measured at 140K: Au_1-C_1 2.031(3), Au_1-C_2 2.034(2), Au_1-N_1 2.163(2), Au_1-N_2 2.137(2), N_1-Au_1-N_2 76.62(7), N_2-Au_1-C2 103.02(9), C_2-Au_1-C_1 80.0(1) C_1-Au_1-N_1 104.32(9).

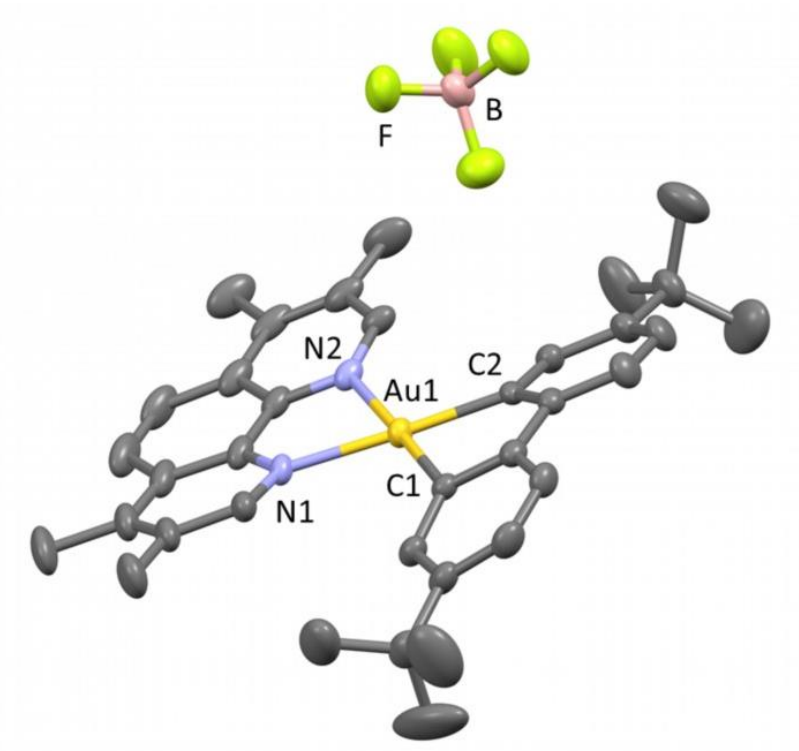

Figure 5: Crystal structure of complex **5a**. Ellipsoids set at 50% probability. Hydrogen atoms and toluene have been omitted for clarity. Selected bond distances [Å] and angles [°] measured at 140K:

Au_1-C_1 2.035(4), Au_1-C_2 2.042(4), Au_1-N_1 2.141(3), Au_1-N_2 2.150(4), N_1-Au_1-N_2 77.3(1), N_2-Au_1-C2 102.3(1), C_2-Au_1-C_1 79.7(2) C_1-Au_1-N_1 100.7(1).

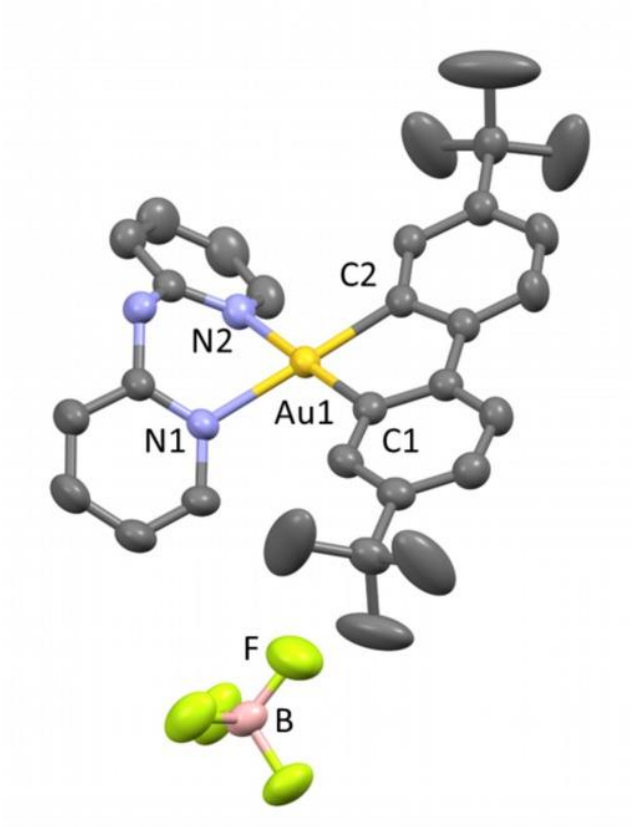

Figure 6: Crystal structure of complex **7**. Ellipsoids set at 50% probability. Hydrogen atoms, toluene and CH_2Cl_2 have been omitted for clarity. Selected bond distances [Å] and angles [°] measured at 140K: Au_1-C_1 2.033(3), Au_1-C_2 2.032(3), Au_1-N_1 2.133(2), Au_1-N_2 2.124(3), N_1-Au_1-N_2 82.25(9), N_2-Au_1-C2 97.7(1), C_2-Au_1-C_1 81.1(1) C_1-Au_1-N_1 98.9(1).

All complexes show a slightly distorted square-planar geometry around the central Au(III) cation. The distortion appears to be less significant in the case of complex **7** due to the larger biting angle provided by the less constrained 6-membered ring. In this particular case, the 6-membered ring adopts a boat-like conformation similar to what was previously observed for (C^N) cyclometallated benzylpyridine Au(III) complexes.[12] Moreover, while $[(C^N^C)Au(L)]^{n+}$ complexes are fully planar,[14,25,26] all $[(C^C)Au(N^N)]^+$ complexes display a distortion to planarity either by bending of the (C^C) ligand as in the case of complexes **2a** and **5a** or by a twisting of the plane of the (N^N) chelate with respect to the plane of the (C^C) chelate as in the case of complexes **1** and **3**. This latter twisting of the (N^N) and (C^C) chelates with respect to each other seems to induce a strong heterogeneity in the length of the Au-N bonds (Au_1-N_1 2.131(7), Au_1-N_2 2.144(7) and Au_1-N_1 2.163(2), Au_1-N_2 2.137(2) for complexes **1** and **3** respectively). These differences in bond length may lead to a lack of symmetry of the compounds which may explain the broadening of the ^{1}H NMR signals for complexes **1** and **3** (see above). Interestingly, Au-N bonds appear longer in the case of the phenanthroline-based complex **5a** than for the bipyridine-based complexes **1** and **2a**. Moreover, complex **3** bearing a 4,4'-(CO_2Me)-2,2'-bipyridine ligand present a Au-N bond significantly longer (2.163(2) Å) than all the other complexes.

Log P measurement

Lipophilicity (or octanol / water partition coefficient, log P) is one of the parameters included in the "Lipinski's rule of five" to evaluate the drug likeness of a molecule.[27] It predicts a reduced absorption for compounds with a Log P value greater than 5. We measured the Log P values of all $[(C^C)Au(N^N)]^+$ complexes following a well-established HPLC-based protocol.[28] Data are provided in table S2. Strong differences could be observed depending of the (N^N) chelate. Complexes with dipyridylamine ligands (complexes **7** and **8**) appear to be the less lipophilic with Log P of 1.37 and 2.15, respectively. Complexes with bipyridine ligands (complexes **1**-**3**) presented Log P values between 1.94 and 2.80, all compliant with Lipinski's rule. Variation of Log P values is the largest for complexes with phenanthroline ligands ranging 1.64 for complex **4** to 9.83 for **5a**. Moreover, as one could have expected, the presence of t-butyl groups on the (C^C) chelate also add to the lipophilicity of the complexes.

In vitro antiproliferative properties.

All complexes appeared to be soluble enough in aqueous media with 1% DMSO at the concentrations used for the antiproliferative assays. To begin with, complexes **1**-**8** were screened against the "triple negative" breast cancer cell line MDA-MB-231 as platinum-based complexes are currently the standard of care for this type of cancer.[29] Evaluation of the mitochondrial activity (correlated to cell proliferation) of MDA-MB-231 cells after 72 h of incubation with complexes **1**-**8** and cisplatin at concentrations of 10 and 1 µM was determined by using the established MTT assay (see the experimental section for details) (figure 7).

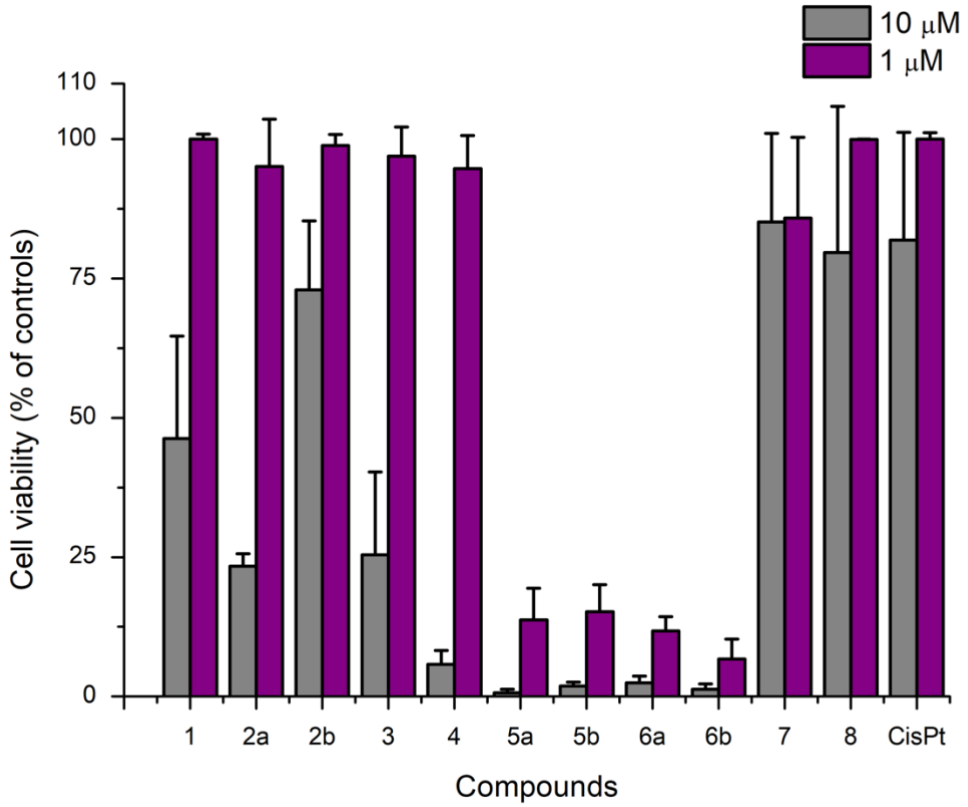

Figure 7: Inhibition of MDA-MB-231 cell growth by complexes **1**-**8** and cisplatin; the cell viability was measured for two concentrations; each data represents the average of three experiments ± standard error.

One can observe the strong impact of the (N^N) ligand on cell viability. Complexes with phenanthroline-based ligands (**4-6**) appear all highly efficient in reducing cell viability (cell viability lower than 15% at a concentration of 1 µM for **5a-b** and **6a-b** and cell viability of 5.8 ± 2.4% at a concentration of 10 µM for **4**), while complexes with bipyridine-based ligands have a reduced impact on cell viability (cell viability of 46 ± 18%; 23 ± 2% and 25 ± 15% at a concentration of 10 µM for **1**, **2a** and **3,** respectively) with complex **2b** being almost inefficient even at the concentration of 10 µM. In the same way, complexes **7** and **8** presenting 2,2'-dipyridylamine-based ligands appeared totally ineffective at both tested concentrations. Moreover, while no discrimination could be observed either between complexes **5a** and **5b n**or between **6a** and **6b**, complex **2a** appears more active than its analog **2b** lacking the t-butyl groups on the (C^C) chelate. This difference can be explained by the reduced solubility of complex **2b** compared to **2a.**

We applied a selection threshold to select only the compounds reducing cell viability by more than 50 % at a concentration of 10 µM. In this manner, we selected seven complexes out of the eleven, namely **2a**, **3**, **4**, **5a-b** and **6a-b** for the following IC_{50} (inhibitory concentration at 50%) measurement on a larger panel of human cancer cell lines. This panel included MDA-MB-231 cells (« triple negative » breast cancer), MCF-7 cells (breast adenocarcinoma) and A2780 cells (ovarian adenocarcinoma). These results were compared to a non-cancerous breast cell line (MCF-10A), the five corresponding (N^N) ligands, **(CNC)Au** and cisplatin. Results are summarized in table 1.

Table 1: Effect of compounds **1**, **2a**, **3**, **4**, **5a-b**, **6a-b**, cisplatin, **(CNC)Au** and the corresponding (N^N) ligands on cell viability of a panel of human cancerous and non-cancerous cell lines after 72 h of incubation at 37 °C; each data represents the average of three experiments ± standard error.

Compounds	**IC_{50} ± sd (µM)**			
	MDA-MB-231	**MCF-7**	**A2780**	**MCF-10A**
2a	1.6 ± 0.3	1.0 ± 0.2	4.8 ± 1.9	0.9 ± 0.1
3	2.0 ± 0.7	1.1 ± 0.9	7.0 ± 2.4	>50
4	1.0 ± 0.1	1.5± 0.2	1.12 ± 0.01	1.2 ± 0.2
5a	0.38 ± 0.03	0.5 ± 0.1	0.21 ± 0.01	0.57 ± 0.07
5b	0.24 ± 0.04	0.26 ± 0.04	0.19 ± 0.01	0.41 ± 0.08
6a	0.17 ± 0.03	0.15 ± 0.01	0.12 ± 0.01	0.54 ± 0.02
6b	0.3 ± 0.1	0.4 ± 0.1	0.17 ± 0.01	0.7 ± 0.2
CisPt[a]	20.4 ± 3.4	14 ± 3.5	1.0 ± 0.2	3.2 ± 0.8
(CNC)Au	0.42 ± 0.03	0.42 ± 0.02	0.03 ± 0.01	0.27 ± 0.03
Me_2Bipy	10.5 ± 0.2	10.6 ± 0.2	12.5 ± 2.3	1.04 ± 0.01
$(MeCO_2)_2$Bipy	>50	>50	>50	>50
Phen	3.2 ± 0.6	2.6 ± 0.6	2.2 ± 0.6	3.4 ± 0.3
Me_4Phen	0.51 ± 0.01	0.7 ± 0.2	0.21 ± 0.07	1.2± 0.4

Ph_2Phen	0.8 ± 0.3	0.8 ± 0.3	0.28 ± 0.06	2.2 ± 0.3

[a] see reference for the IC_{50} values of cisplatin[30]

All the $[(C^C)Au(N^N)]^+$ complexes appear to be active in a low micromolar to sub-micromolar range on the three cancer cell lines. As already observed in the previous screening, phenanthroline-based complexes (**4**, **5b, 5b, 6a** and **6b**) are more efficient in reducing cell proliferation than the bipyridine-based complexes (**2a**, **3**). All the $[(C^C)Au(N^N)]^+$ complexes are more potent than cisplatin toward the two breast cancer cell lines, whereas only **2a** and **3** present less potency than cisplatin on A2780. Complex **6a** demonstrated particularly strong antiproliferative effects with IC_{50} values of 0.17 ± 0.03 µM, 0.15 ± 0.01 µM and 0.12 ± 0.01 µM on MDA-MB-231, MCF-7 and A2780 cells, respectively. This makes **6a** between 8.3 and 120 times more efficient than cisplatin. Complex **6a** also appears very active toward the non-cancerous cell line MCF-10A with an IC_{50} value of 0.54 ± 0.02 µM, resulting in a selectivity index of 3.6 with respect to MCF-7. Moreover, as noticed for complexes **2a** and **2b**, **6a** shows more activity than its analog **6b** where the (C^C) chelate lacks the ^{t}Bu substituents. Finally, **6a** is more active than **(CNC)Au** on MDA-MB-231 and MCF-7 while it is 4 times less efficient than **(CNC)Au** on A2780 cells. Nearly all the newly formed complexes as well as **(CNC)Au** are equally toxic to the non-cancerous cell line MCF-10A except for complex **3**. This complex shows a moderate cytotoxic activity to MDA-MB-231, MCF-7 and A2780 cells with IC_{50} = 2.0 ± 0.7, 1.1 ± 0.9 and 7.0 ± 2.4 µM, respectively while no effect on cell proliferation is noticed for MCF-10A up to a concentration of 50 µM. Collectively, these data point out to a probably different mechanism of action of the $[(C^C)Au(N^N)]^+$ complexes compared to cisplatin and **(CNC)Au**.

Altogether and regardless of the cell line, there appears to be a general correlation between the activity of the gold complexes and their corresponding ligands. In the Phen and Ph_2Phen series, the complexes are 2 to 5 times more active than the composite ligands. In contrast, the Me_4Phe complexes are as active as the corresponding ligand. For these three series, a relatively good homogeneity is noticed between the cell lines. In comparison, the Me_2bpy complexes are 1.6 to 10.6 times more efficient than the corresponding ligand and a high heterogeneity is noticed between the tested cell lines.

These data suggest that, while the antiproliferative effects of complex **6a** mainly come from the (N^N) ligand Ph_2Phen with a small contribution of the gold atom, the activity of complex **3** is exclusively due to the presence of the gold center.

Reactivity toward biomolecules.

Prior to the experimental investigation of the reactivity of the $[(C^C)Au(N^N)]^+$ complexes with biomolecules, we calculated the energetic parameters for complexes **1-8** using DFT at the (BPW91/6-31g(d,p) (others) Au(SDD+f) level of theory. In the case of Au(III), ligand substitution can only occur *via* a dissociative mechanism, we calculated the bond dissociation energies (BDE, table S2) of the (N^N) chelates for all $[(C^C)Au(N^N)]^+$ complexes. Among complexes carrying ^{t}Bu substituents on the (C^C) ligand (complexes **1-4**, **5a**, **6a** and **7-8**), no major differences could be observed in the BDEs except for complexes **3** and **8**, which show a BDE 8 kcal/mol lower than all other complexes. This is in line with the data obtained in the solid state by X-Ray diffraction in which no major differences in Au-N bond lengths have been observed except for **3** which showed a particularly longer Au-N bond. This suggests

that a similar reactivity toward biomolecules could be expected. Complexes without ^{t}Bu groups on the (C^C) chelate appear to have BDEs greater by 5.5 kcal/mol which may account in part for the slightly lower antiproliferative activity observed for **2b** and **6b** with respect to **2a** and **6a**.

Complexes **3** and **6a** were further selected for the reactivity studies as the two most interesting candidates identified from the antiproliferative assay. Both complexes were incubated for 24 h at 37 °C alone in DMSO. No de-coordination of the (N^N) ligands took place, indicating that both complexes were stable in these conditions (figure S3 and S4). Further, complexes **3** and **6a** were treated with one equivalent of several amino acids presenting different coordinative functions including cysteine (thiol), methionine (thioether), histidine (imidazole) and serine (alcohol) as well as guanine, either one by one or in mixture to establish a selectivity between the reagents.

Reaction mixtures were analyzed by low resolution mass spectrometry to establish whether or not the complexes reacted with the biomolecules and the adducts were then identified by high resolution mass spectrometry (see experimental part for details). Results are depicted in figures S1 and S2. Both complexes appear to display a rather similar reactivity pattern since no reaction occurs with methionine and serine. In contrast, adducts are formed upon reaction of cysteine and histidine, both in the single component experiments and in the mixture experiments, leading in each case to the replacement of the (N^N) ligand by the amino acid with maintenance of the [(C^C)Au] moiety and the +III oxidation state as could be concluded by the isotopic pattern and the monocationic charge of the resulting adducts. This suggests that cysteine and histidine residues of proteins may be the main interaction points of this class of compounds and rule out direct coordination to DNA as previously reported for other Au(III) complexes.[31] This result is consistent with the $[(C^C)Au(N^N)]^+$ complexes having a mode of action distinct from cisplatin.

Based on these results, complexes **3**, **6a** and **(CNC)Au** were incubated with glutathione (GSH), a tripeptide present at a millimolar level in cells and responsible for redox balance maintenance and xenobiotic detoxification.[32] Furthermore, GSH is involved in resistance to platinum drugs[33] and is known to reduce Au(III) complexes to Au(I) or Au(0) leading to their deactivation.[34,35] After reaction of complexes **3**, **6a** and **(CNC)Au** with 0, 1, 2 and 5 equivalents of GSH in a 1/1 DMSO/PBS mixture for 24 h at 37 °C, the reaction mixtures were analyzed by low resolution mass spectrometry (figures 8, S5 and S6). The presence of PBS in the reaction medium did not lead to decomposition of complexes **3**, **6a** and **(CNC)Au** suggesting their stability in aqueous environment. For both $[(C^C)Au(N^N)]^+$ complexes **3** and **6a**, reaction with increasing amount of GSH leads to the progressive disappearance of the molecular peak and the appearance of a peak corresponding to adducts having a 1/1 stoichiometry between GSH and the $[(C^C)Au]^+$ moiety. High resolution mass spectrometry revealed that these adducts were doubly charged species, whose structure was attributed to a S-bridged dimer or a monomeric structure with a chelating GS^{2-} depending of the protonation state of the side chains of GSH as depicted in figures 10 and S3. Substitution of the (N^N) ligand by one GSH molecule is consistent with previous observations for (C^N) cyclometallated Au(III) complexes[36] leading in both cases to neutral Au(III) entities. Furthermore, as previously shown for a similar compound,[15] no reaction between complex **(CNC)Au** and GSH was observed (figure S4) highlighting the tremendous increase of reactivity toward biomolecules due to the reorganization of the coordination sphere moving from the $[(C^N^C)Au(NHC)]^+$ scaffold to the $[(C^C)Au(N^N)]^+$ one.

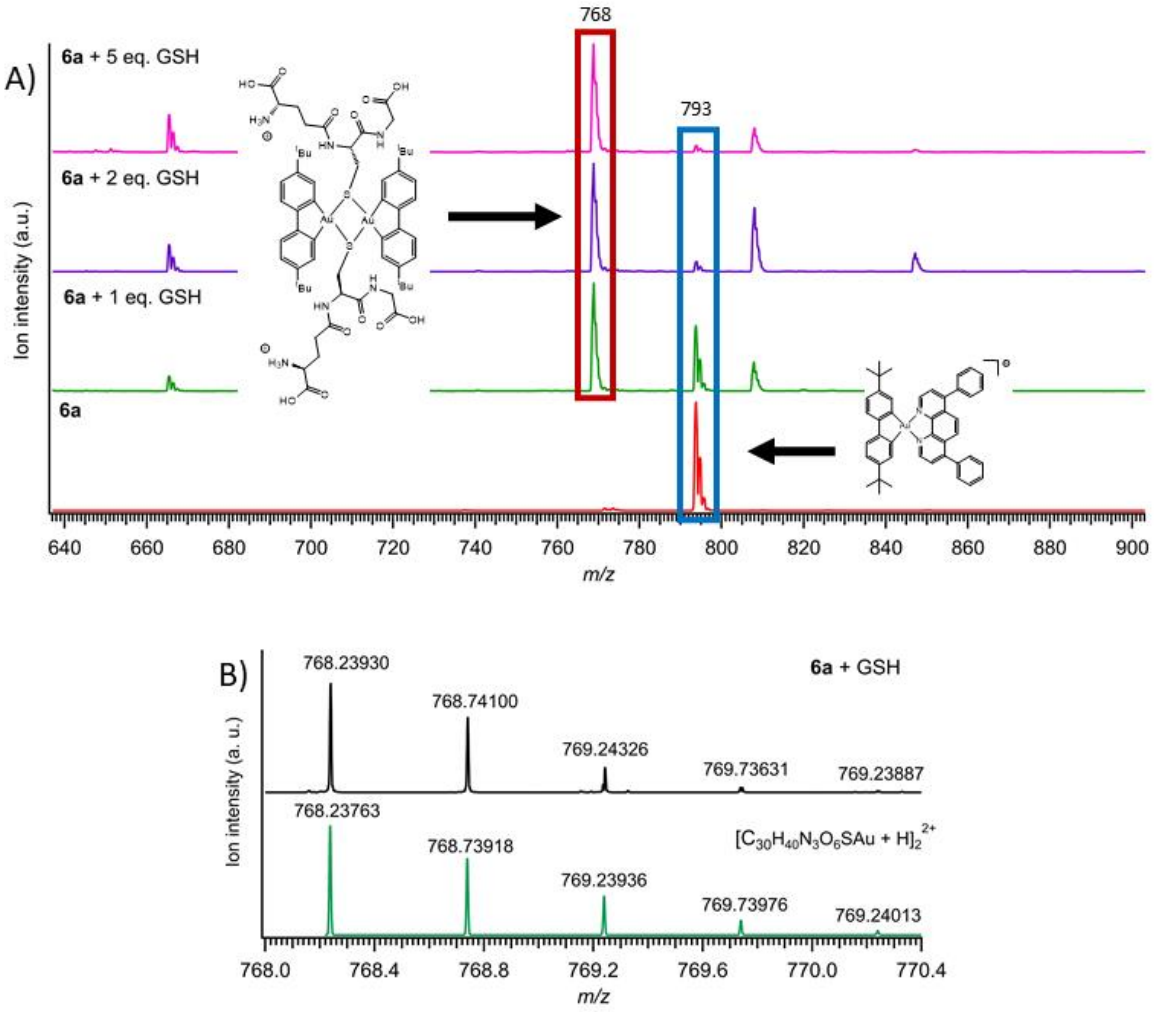

Figure 8: A) Low resolution mass spectra of mixtures of complex **6a** and 0, 1, 2 or 5 equivalents of GSH after 24 h at 37 °C in DMSO/PBS 1:1 and B) identification of the formed adduct by high resolution mass spectrometry.

Upon reaction of cysteine, histidine or GSH with the complexes, one equivalent of ligand is released. Since the phenanthroline ligands have a marked effect on cell proliferation on their own, part of the cytotoxicity reported above is likely due to the ligands themselves.

Uptake studies.

Metal uptake is recognized as an important parameter in the antiproliferative activity of metal-based drug candidates. Indeed, a lower platinum uptake has been observed in cisplatin-resistant tumors.[37] In the same way, higher accumulation of gold complexes has sometimes been correlated with higher cytotoxicity.[15,35] Uptake measurements were performed by treating A2780 cells with 5 µM complexes **3**, **4**, **6a** and **6b** at 37 °C for 2 h, as the largest differences in IC_{50} have been determined between these complexes on this cell line. Incubation was carried out in the presence and in the absence of fetal bovine serum (FBS) in the culture medium in order to assess the impact of serum proteins, such as albumin, on the uptake of the complexes (see experimental part for details). The intracellular gold concentration was quantified by high-resolution continuum source atomic absorption spectroscopy (HRCS-AAS). Results are presented in figure 9. For all tested complexes, the uptake appears to be strongly reduced when the compounds were incubated in the presence of FBS. This feature is especially pronounced for the three complexes carrying the diterbutylphenyl ligand (complexes **3**, **4**

and **6a**). This suggests that serum proteins may act as sequestrators for these $[(C^C)Au(N^N)]^+$ complexes leading to a reduced accumulation with the cancer cells. Such a behavior has already been reported for other organogold complexes.[38] Moreover, the intracellular concentration of gold in cells under FBS-containing conditions is mostly independent on the complex structure although the IC_{50} spanned from 0.12 to 7 µM and log P ranged from 1.64 to 5.54. Thus the difference of antiproliferative activity between the complexes may at least partly result from the intrinsic toxicity of the (N^N) ligands released from the $[(C^C)Au(N^N)]^+$ complexes upon their interaction with biomolecules in the extracellular or the intracellular medium.

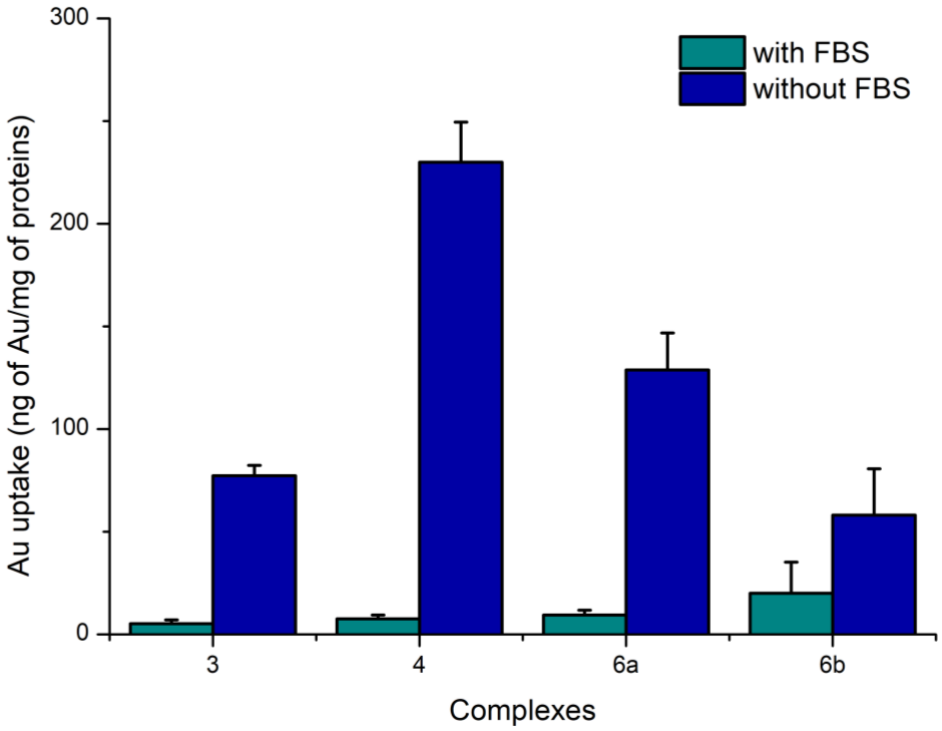

Figure 9: Gold uptake (in ng/mg of proteins) in A2780 cells treated with 5 µM complexes **3**, **4**, **6a** and **6b** for 2 h at 37 °C in culture medium with or without 10% FBS (v/v).

Interactions with higher order DNA structures and thioredoxin reductase inhibition study.

Although Au complexes are known not to target DNA,[3],[5] cyclometalated Au(III) complexes have been reported to efficiently stabilize higher order DNA structures such as G-quadruplexes and i-motif structures.[15,39,40] The $[(C^C)Au(N^N)]^+$ complexes were screened as potential stabilizers of a panel of G-quadruplex structures (NasT, hTeloG and NRF2), an i-motif structure (DAP) and classical double-stranded DNA (DS) using a FRET-melting protocol (see experimental part for details). Contrarily to what has been observed for $[(C^N^C)AuL]^+$ complexes, none of the $[(C^C)Au(N^N)]^+$ complexes stabilize any of the tested DNA structures (Figure S8). Such a different behavior may be explained by the lack of planarity of the $[(C^C)Au(N^N)]^+$ structures as observed previously in the solid state structures, preventing π-stacking interactions with the accessible tetrads of the G-quadruplexes or intercalation.

The intracellular role of thioredoxin reductase (TrxR) consists in reducing thioredoxin (Trx) in an NADPH-dependent manner. Thioredoxin in turn reduces different proteins including peroxiredoxin

(involved in the regulation of cellular level of hydrogen peroxide). It's active site is composed of a cysteine and a selenocysteine residues. TrxR has been reported as a potential intracellular target of gold complexes[41] and in particular several cyclometalated gold(III) complexes.[14,35] Based on these data and the strong reactivity of our $[(C^C)Au(N^N)]^+$ complexes with GSH, our two most promising complexes **3** and **6a** as well as the cyclometallated complex **(CNC)Au** were tested as inhibitors of mammalian TrxR *in vitro* (table 2).

Table 2: Effect of complexes **3**, **6a** and **(CNC)Au** on mammalian TrxR activity *in vitro*.

Complexes	IC_{50} (μM)
3	9.5 ± 0.1
6a	1.2 ± 0.1
(CNC)Au	8.8 ± 1.1

Interestingly, all three complexes present IC_{50} values in the micromolar range, higher than their respective IC_{50} values against cancer cells. This finding markedly contrasts with the previously reported nanomolar inhibition activity of [(C^N^C)AuX] and [(C^N^C)AuL]+ complexes.[14,18] This suggests than TrxR may not be the main target of this class of organogold complexes.

Conclusions

We have synthesized a series of eleven new organometallic gold(III) complexes bearing a (C^C) biphenyl-based ligand and a bipyridine-, phenanthroline- or dipyridylamine-based (N^N) ligand with yields higher than 80 %. The complexes were fully characterized and the molecular structure of complexes **1**, **2a**, **3**, **5a** and **7** was confirmed by X-Ray diffraction. The analysis of the crystallographic structures revealed the non-planarity of the complexes either by bending of the (C^C) ligand or by twisting of the (N^N) ligand with respect to the [(C^C)Au] plane. The antiproliferative studies highlighted complexes **3** and **6a** as particularly promising as they appeared more selective and more active than the reference compounds **(CNC)Au** and cisplatin. Complexes **3** and **6a** remained stable upon incubation for 24 h at 37 °C in DMSO and PBS while substitution of the (N^N) ligands by histidine and cysteine to form $[(C^C)Au^{III}(Hist/Cys)]$ complexes was observed. Incubation of the complexes in the presence of GSH also resulted in the substitution of the (N^N) ligands to form 1/1 adducts between the $[(C^C)Au]^+$ fragment and GSH either as a monomer with a chelating GSH or as a GSH-bridged dimer depending on the protonation state of GSH. Again the +III oxidation state of the gold center was retained. Formation of these adducts was concomitant with the release of the (N^N) ligand. In the same conditions and as previously observed by ^{1}H NMR, **(CNC)Au** was fully inert in the presence of GSH.

Uptake studies of complexes **3**, **4**, **6a** and **6b** in A2780 cells revealed a low uptake of the complexes due to sequestration of the complexes by serum proteins. In addition, intracellular gold concentration was independent of complex structure and partition coefficient. Taken together, the antiproliferative properties of **3** are only due to the gold center as the corresponding (N^N) ligand is not toxic. Conversely, the antiproliferative properties of **6a** seem to partly originate from the release of the highly toxic bathophenanthroline ligand.

Activity of the $[(C^C)Au(N^N)]^+$ complexes was tested against higher order DNA structures such as G-quadruplexes and i-motif as $[(C^N^C)Au(NHC)]^+$ complexes are known to stabilize these structures and inhibit TrxR. Interestingly, in both cases, our $[(C^C)Au(N^N)]^+$ complexes appeared to only poorly interact with these potential biological targets, which suggests that the involvement of these targets in the mechanism of action of the $[(C^C)Au(N^N)]^+$ complexes could be ruled out.

To conclude, these data highlight the potential of reorganizing the coordination sphere of the well-known $[(C^N^C)AuL]^+$ scaffold using biphenyl-based (C^C) ligands. We demonstrated that $[(C^C)Au(N^N)]^+$ complexes have a very different reactivity with respect to $[(C^N^C)Au(NHC)]^+$ complexes, making them a new class of organometallic Au(III) anticancer drug candidates whose mechanism of action will have to be studied more thoroughly. These investigations are ongoing in the lab.

Experimental part

General remarks.

All reactions and manipulations were carried out under an argon atmosphere using standard Schlenk techniques. Anhydrous solvents were obtained by standard procedures. Chemicals were purchased from various manufacturers and used as received. ^1H and ^{13}C NMR spectra were acquired on a Bruker 400 MHz spectrometer. Chemical shifts (δ) are expressed as ppm referenced to the solvent residual signal. Splitting patterns are expressed as follows: s, singlet; d, doublet; t, triplet; m, multiplet. Mass spectrometry was carried out at the HRMS facility of Sorbonne Université (Paris). High resolution mass spectra (HR-MS) were recorded on a LTQ-Orbitrap XL mass spectrometer (Thermo Scientific, San Jose, CA, USA). IR spectra were recorded on a Tensor 27 FT-IR spectrometer (Bruker). Elemental analysis was performed at the elemental analysis service of ICSN (Gif-sur-Yvette, France). Dimeric gold precursors as well as ligands N-ethyl-2,2'-dipyridylamine have been synthesized according to reported procedures.[21,42] Ligands have been purchased at Sigma-Aldrich or Fluorochem and used as received.

Synthesis of 1, 2a, 3, 4, 5a, 6a, 7, 8

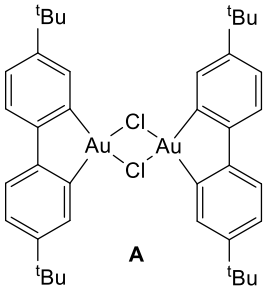

A

To a suspension of dimer **A** in CH_2Cl_2 (3 mL) was added 2 equivalents of the appropriate ligand. Once the solubility reached (after 20 min), a solution of $AgBF_4$ (2 equivalents) in MeCN (1 mL) was added. Precipitation occurs immediately. The mixture was left to stir at room temperature for ca. 2 h and subsequently passed through a pad of celite. The filtrate was taken to dryness, then crystallized in DCM/Pentane and dried.

1: **A** (40.0 mg, 0.04 mmol) and **2,2'-Bipyridine** (12 mg, 0.08 mmol) afford a white powder (54 mg, 0.08

mmol, 97% yield). ^{1}H NMR (400 MHz, MeCN-d_3, 298K): δ 1.38 (s, 18 H, tBu), 7.41 (m, 4 H, $H^{4/5}$), 7.51 (s, 2H, H^{2}), 8.03 (m, 2H, H^{8}), 8.45 (m, 2H, H^{9}), 8.63 (d, $^{3}J_{H\text{-}H}$ = 8 Hz, 2H, H^{10}), 9.17 (s, 2H, H^{7}). ^{13}C{^{1}H} Jmod (MeCN-d_3, 100 MHz, 298 K): δ 31.5 (s, *CH₃tBu*), 36.0 (s, C^{tBu}), 123.1 (s, $C^{4/5}$), 126.1 (s, C^{10}), 127.2 (s, $C^{4/5}$), 128.1 (s, C^{2}), 129.3 (s, C^{8}), 143.6 (s, C^{9}), 150.6 (s, C^{1}), 150.9 (s, C^{7}), 151.7 (s, C^{3}), 154.8 (s, C^{6}), 156.0(s, C^{11}). ESI-MS (MeCN) *positive mode exact mass* for $[C_{30}H_{32}AuN_2]^+$ (617.2231): measured *m/z* 617.2226 $[M\text{-}BF_4]^+$. Calcd for $C_{30}H_{32}AuBF_4N_2.0.5\ H_2O$ (704.3702): C, 50.51; H, 4.66; N, 3.93. Found: C, 50.36; H, 4.43; N, 3.77.

2a: **A** (40.0 mg, 0.04 mmol) and **4,4-Dimethyl-2,2-bipyridine** (15 mg, 0.08 mmol) afford a white powder (48 mg, 0.07 mmol, 84% yield). ^{1}H NMR (400 MHz, MeCN-d_3, 298K): δ 1.37 (s, 18 H, tBu), 2.66 (s, 6H, CH_3), 7.40 (m, 4 H, $H^{4/5}$), 7.50 (s, 2H, H^{2}), 7.87 (d, $^{3}J_{H\text{-}H}$ = 5.6 Hz, 2H, H^{8}), 8.49 (s, 2H, H^{10}), 9.02 (d, $^{3}J_{H\text{-}H}$ = 5.6 Hz, 2H, H^{7}). ^{13}C{^{1}H} Jmod (MeCN-d_3, 100 MHz, 298 K): δ 21.9 (s, CH_3), 31.5 (s, *CH₃tBu*), 35.9 (s, C^{tBu}), 123.1 (s, $C^{4/5}$), 126.8 (s, C^{10}), 127.0 (s, $C^{4/5}$), 128.0 (s, C^{2}), 130.0 (s, C^{8}), 149.8 (s, C^{7}), 150.6 (s, C^{1}), 151.6 (s, C^{3}), 154.5 (s, C^{6}), 155.7 (s, C^{11}), 157.0 (s, C^{9}). ESI-MS (MeCN) *positive mode exact mass* for $[C_{32}H_{36}AuN_2]^+$ (645.2544): measured *m/z* 645.2536 $[M\text{-}BF_4]^+$. Calcd. for $C_{32}H_{36}AuBF_4N_2$ (732.2573): C, 52.48; H, 4.95; N, 3.82. Found: C, 52.40; H, 4.90; N, 3.64.

3: **A** (40.0 mg, 0.04 mmol) and **Dimethyl 2,2-bipyridine-4,4-dicarboxylate** (22 mg, 0.08 mmol) afford a yellow powder (53 mg, 0.06 mmol, 83% yield). ^{1}H NMR (400 MHz, MeCN-d_3, 298K): δ 1.38 (s, 18 H, tBu), 4.06 (s, 6 H, CH_3), 7.43 (m, 4 H, $H^{4/5}$), 7.48 (s, 2H, H^{2}), 8.42 (s, 2H, H^{8}), 9.12 (s, 2H, H^{10}), 9.26 (s, 2H, H^{7}). ^{13}C{^{1}H} Jmod (MeCN-d_3, 100 MHz, 298 K): δ 31.5 (s, *CH₃tBu*), 36.0 (s, C^{tBu}), 54.3 (s, CH_3), 123.3 (s, $C^{4/5}$), 125.6 (s, C^{10}), 127.4 (s, $C^{4/5}$), 127.9 (s, C^{2}), 128.6 (s, C^{8}), 143.7 (s, C^{9}), 150.4 (s, C^{1}), 152.0 (s, C^{3}), 155.1 (s, C^{6}), 156.3 (s, C^{11}), 164.4 (s, C^{12}). ESI-MS (MeCN) *positive mode exact mass* for $[C_{34}H_{36}AuN_2O_4]^+$ (733.2341): measured *m/z* 733.2334 $[M\text{-}BF_4]^+$. Calcd for $C_{34}H_{36}AuBF_4N_2O_4.H_2O$ (820.4422): C, 48.71; H, 4.57; N, 3.34. Found: C, 48.98; H, 4.52; N, 3.07.

4: **A** (40.0 mg, 0.04 mmol) and **1,10-phenanthroline** (14 mg, 0.08 mmol) afford a yellow powder (49.8 mg, 0.07 mmol, 86% yield). ^{1}H NMR (400 MHz, MeCN-d_3, 298K): δ 1.35 (s, 18 H, tBu), 7.34 (s, 4 H, $H^{4,5}$), 7.52 (s, 2H, H^{2}), 8.31 (m, 4H, $H^{8,12}$), 8.98 (d, $^{3}J_{H\text{-}H}$ = 8 Hz, 2H, H^{9}), 9.46 (d, $^{3}J_{H\text{-}H}$ = 4.8 Hz, 2H, H^{7}). ^{13}C{^{1}H} Jmod (MeCN-d_3, 100 MHz, 298 K): δ 31.6 (s, *CH₃tBu*), 36.1 (s, C^{tBu}), 123.2 (s, $C^{4/5}$), 127.1 (s, $C^{4/5}$), 127.7 (s, C^{12}), 128.3 (s, C^{2}), 129.5 (s, C^{8}), 132.4 (s, C^{10}), 142.8 (s, C^{9}), 145.9 (s, C^{11}), 150.7 (s, C^{1}), 151.5 (s, C^{7}), 151.7 (s, C^{3}), 154.4 (s, C^{6}). ESI-MS (MeCN) *positive mode exact mass* for $[C_{32}H_{32}AuN_2]^+$ (641.2231): measured *m/z* 641.2225 $[M\text{-}BF_4]^+$. Calcd for $C_{32}H_{32}AuBF_4N_2$ (728.395): C, 52.77; H, 4.43; N, 3.85. Found: C, 52.62; H, 4.36; N, 3.86.

5a: **A** (40.0 mg, 0.04 mmol) and **3,4,7,8-Tetramethyl-1,10-phenanthroline** (19 mg, 0.08 mmol) afford grey powder (46.1 mg, 0.06 mmol, 83% yield). ^{1}H NMR (400 MHz, MeCN-d_3, 298K): δ 1.41 (s, 18 H, tBu), 2.72 (s, 6 H, CH_3), 2.92 (s, 6 H, CH_3), 7.41 (m, 4 H, $H^{4,5}$), 7.64 (s, 2H, H^{2}), 8.47 (s, 2H, H^{12}), 9.33 (s, 2H, H^{7}). ^{13}C{^{1}H} Jmod (MeCN-d_3, 100 MHz, 298 K): δ 16.1 (s, CH_3), 18.7 (s, CH_3), 31.6 (s, *CH₃tBu*), 36.0 (s, C^{tBu}), 123.0 (s, $C^{4/5}$), 125.7 (s, $C^{4/5}$), 126.8 (s, C^{12}), 128.31(s, C^{2}), 131.0 (s, C^{8}), 136.7 (s, C^{10}), 144.6 (s, C^{11}), 150.6 (s, C^{1}), 151.1 (s, C^{7}), 151.4 (s, C^{3}), 152.1 (s, C^{9}), 154.0 (s, C^{6}). ESI-MS (MeCN) *positive mode exact mass* for $[C_{36}H_{40}AuN_2]^+$ (697.2857): measured *m/z* 697.2850 $[M\text{-}BF_4]^+$. Calcd for $C_{36}H_{40}AuBF_4N_2.0.5\ H_2O$ (784.5002): C, 54.49; H, 5 .21; N, 3.53. Found: C, 54.44; H, 5.11; N, 3.16.

6a: **A** (40.0 mg, 0.04 mmol) and **4,7-Diphenyl-1,10-phenanthroline** (26 mg, 0.08 mmol) afford a yellow/orange powder (60.3 mg, 0.07 mmol, 87% yield). ^{1}H NMR (400 MHz, MeCN-d_3, 298K): δ 1.39 (s, 18 H, tBu), 7.40 (m, 4 H, $H^{4/5}$), 7.61 (s, 2H, H^{2}), 7.70 (m, 10H, $H^{14,15,16}$), 8.28 (m,4H, $H^{8,12}$), 9.54 (d, $^{3}J_{H\text{-}H}$ = 5.2 Hz, 2H, H^{7}). ^{13}C{^{1}H} Jmod (MeCN-d_3, 100 MHz, 298 K): δ 31.5 (s, *CH₃tBu*), 36.0 (s, C^{tBu}), 122.8 (s, $C^{4/5}$),

126.9 (s, $C^{4/5}$), 127.2 (s, C^{12}), 127.9 (s, C^{2}), 128.1 (s, C^{8}), 130.0 (s, C^{13}), 130.1 (s, $C^{14/15}$), 130.9 (s, $C^{14/15}$), 131.3 (s, C^{16}), 135.9 (s, C^{10}), 146.0 (s, C^{11}), 150.2 (s, C^{1}), 151.4 (s, C^{7}), 151.6 (s, C^{3}), 154.3 (s, C^{9}), 154.5 (s, C^{6}). ESI-MS (MeCN) *positive mode exact mass* for $[C_{44}H_{40}AuN_2]^+$ (793.2857): measured *m/z* 793.2856 $[M\text{-}BF_4]^+$. Calcd for $C_{44}H_{40}AuBF_4N_2$ (880.5882): C, 60.01; H, 4.58; N, 3.18. Found: C, 59.99; H 4.81; N 4.06.

7: **A** (30.0 mg, 0.03 mmol) and **2,2'-Dipyridylamine** (10 mg, 0.06 mmol) afford a white powder (40.0 mg, 0.06 mmol, 93% yield). ^{1}H NMR (400 MHz, MeCN-d_3, 323K): δ 1.29 (s, 18 H, tBu), 6.93 (s, 2 H, H^2), 7.36 (m, 4H, $H^{4/5}$), 7.64 (m, 4H, $H^{8/10}$), 8.18 (m, 2H, H^9), 8.60 (m, 2H, H^7), 9.06 (s, 1H, NH). ESI-MS (MeCN) *positive mode exact mass* for $[C_{30}H_{33}AuN_3]^+$ (632.2340): measured *m/z* 632.2333 $[M\text{-}BF_4]^+$. Due to solubility limitations, no $^{13}C\{^1H\}$ NMR spectrum could be recorded. Calcd for $C_{30}H_{33}AuBF_4N_3.1.5H_2O$ (719.3852): C, 48.86; H, 4.78; N, 5.70. Found: C, 48.82; H, 4.40; N, 6.65.

8: **A** (40.0 mg, 0.04 mmol) and **N-Ethyl-2,2'-Dipyridylamine** (16 mg, 0.08 mmol) afford white powder (50 mg, 0.07 mmol, 85% yield). ^{1}H NMR (400 MHz, MeCN-d_3, 298K): δ 1.25 (s, 18 H, tBu), 1.32 (t, $^3J_{H\text{-}H}$ = 6.8 Hz, 3H, CH_3), 4.13 (q, $^3J_{H\text{-}H}$ = 7.1 Hz, CH_2), 6.97 (s, 2 H, H^2), 7.33 (m, 4H, $H^{4/5}$), 7.67 (t, $^3J_{H\text{-}H}$ = 6.4 Hz, 2H, H^8), 7.76 (d, $^3J_{H\text{-}H}$ = 8.4 Hz, 2H, H^{10}), 8.26 (t, $^3J_{H\text{-}H}$ = 7.2 Hz, 2H, H^9), 8.63 (d, $^3J_{H\text{-}H}$ = 5.48 Hz, 2H, H^7). $^{13}C\{^1H\}$ Jmod (MeCN-d_3, 100 MHz, 298 K): δ 13.4 (s, CH_3), 31.4 (s, *CH_3tBu*), 35.9 (s, *C^{tBu}*), 45.31 (s, CH_2), 119.2 (s, C^{10}), 122.6 (s, $C^{4/5}$), 124.2(s, C^8), 126.8 (s, $C^{4/5}$), 129.6 (s, C^2), 144.7 (s, C^9), 149.8 (s, C^7), 150.5 (s, C^1), 150.7 (s, C^3), 151.0 (s, C^6), 155.9 (s, C^{11}). ESI-MS (MeCN) *positive mode exact mass* for $[C_{32}H_{37}AuN_3]^+$ (660.2653): measured *m/z* 660.2647 $[M\text{-}BF_4]^+$. Calcd for $C_{32}H_{37}AuBF_4N_3$ (747.4392): C, 51.42; H, 4.99; N, 5.62. Found: C, 51.79; H, 5.08; N, 5.56.

Synthesis of 2b, 5b, 6b

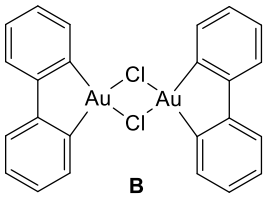

B

To a suspension of **B** in MeCN (3 mL) was added 2 equivalents of the appropriate ligand. Thereafter, a solution of $AgBF_4$ in MeCN (10 ml) was added. The mixture was left to stir at room temperature overnight and after addition of MeCN (40 mL), the suspension was passed through a pad of celite. The filtrate was taken to dryness.

2b: **B** (12.0 mg, 0.014 mmol) and **4,4-Dimethyl-2,2-bipyridine** (5 mg, 0.028 mmol) afford white a powder (16 mg, 0.026 mmol, 92% yield). ^{1}H NMR (400 MHz, MeCN-d_3, 298K): δ 2.60 (s, 6H, CH_3), 7.02 (m, 2 H, H^3), 7.25 (m, 2H, H^2), 7.40 (m, 4H, $H^{4/5}$), 7.65 (d, $^3J_{H\text{-}H}$ = 4.72 Hz, H^8), 8.30 (s, 2H, H^{10}), 8.84 (d, $^3J_{H\text{-}H}$ = 5.6 Hz, 2H, H^7). Due to solubility limitations, no $^{13}C\{^1H\}$ NMR spectrum could be recorded. ESI-MS (MeCN) *positive mode exact mass* for $[C_{24}H_{20}AuN_2]^+$ (533.1292): measured *m/z* 533.1292 $[M\text{-}BF_4]^+$. Calcd for $C_{24}H_{20}AuBF_4N_2$ (620.2082): C, 46.48; H, 3.25; N, 4.52. Found: C, 46.20; H, 3.46; N, 4.25.

5b: **B** (40.0 mg, 0.05 mmol) and **3,4,7,8-Tetramethyl-1,10-phenanthroline** (22 mg, 0.09 mmol) afford off-white powder (59 mg, 0.09 mmol, 94% yield). ^{1}H NMR (400 MHz, MeCN-d_3, 298K): δ 2.60 (s, 6 H, CH_3), 2.82 (s, 6 H, CH_3), 6.98 (m, 6 H, $H^{3/4/5}$), 7.36 (m 2H, H^2), 8.33 (s, 2H, H^{12}), 8.93 (s, 2H, H^7). Due to solubility limitations, no $^{13}C\{^1H\}$ NMR spectrum could be recorded. ESI-MS (MeCN) *positive mode exact mass* for $[C_{28}H_{24}AuN_2]^+$ (585.1600): measured *m/z* 585.1598 $[M+H]^+$. Calcd for $C_{28}H_{24}AuBF_4N_2.6H_2O$

(672.2842): C, 43.10; H, 4.65; N, 3.59. Found: C, 43.00; H, 3.22; N, 3.81.

6b: **B** (40.0 mg, 0.05 mmol) and **4,7-Diphenyl-1,10-phenanthroline** (31 mg, 0.09 mmol) afford yellow powder (67 mg, 0.09 mmol, 93% yield). ^{1}H NMR (400 MHz, MeCN-d_3, 298K): δ 7.01 (m, 4 H, $H^{4/5}$), 7.52 (m, 2 H, H^2), 7.68 (s, 12H, $H^{3/14/15/16}$), 8.09 (m, 4H, $H^{8/12}$), 9.32 (m, 2H, H^7). ESI-MS (MeCN) *positive mode exact mass* for $[C_{36}H_{24}AuN_2]^+$ (681.1600): measured *m/z* 681.1599 $[M\text{-}BF_4]^+$. Calcd for $C_{36}H_{24}AuBF_4N_2.3H_2O$ (768.3722): C, 52.58; H, 3.68; N, 3.41. Found: C, 52.57; H, 3.32; N, 3.62.

X-Ray crystal structure determination for 1, **2a**, **3**, **5a** and **7.** Single crystals were selected, mounted and transferred into a cold nitrogen gas stream. Intensity data was collected with Bruker Kappa-APEX2 systems using fine-focus sealed tube Mo-Kα radiation (**1, 2a, 5a**) or micro-source Cu-Kα radiation (**7, 3**). Unit-cell parameters determination, data collection strategy, integration and absorption correction were carried out with the Bruker APEX2 suite of programs. The structures were solved with SHELXT and refined anisotropically by full-matrix least-squares methods with SHELXL using WinGX (**1, 7, 3**) or Olex2 (**2a, 5a**). **1** was refined as a 2-component perfect inversion twin. PLATON SQUEEZE was used for the final refinement cycles of **2a** to account for undetermined disordered solvent. **5a** was integrated and refined as a 2-component twin. The structures were deposited at the Cambridge Crystallographic Data Centre with numbers CCDC 2057826-2057830 and can be obtained free of charge via www.ccdc.cam.ac.uk.

Crystal data for 1. $C_{30}H_{32}AuBF_4N_2$, orthorhombic $Pca2_1$, a = 14.2695(3) Å, b = 22.7874(4) Å, c = 34.4332(6) Å, α = β = γ = 90°, V = 11196.5(4) Å^3, Z = 16, yellow needle 0.45 × 0.15 × 0.1 mm^3, μ = 5.304 mm^{-1}, min / max transmission = 0.19 / 1.00, T= 200(1) K, λ = 0.71073 Å, θ range = 0.90° to 28.70°, 56210 reflections measured, 25373 independent, R_{int} = 0.0271, completeness = 0.999, 1369 parameters, 61 restraints, Flack x = 0.5, final R indices R1 [I>2σ(I)] = 0.0345 and wR2 (all data) = 0.0786, GOF on F^2 = 1.028, largest difference peak / hole = 1.10 / -0.99 e·Å^{-3}.

Crystal data for 2a. $C_{35.5}H_{40}AuBF_4N_2$, monoclinic C 2/m, a = 21.7197(10) Å, b = 30.3228(14) Å, c = 12.6944(6) Å, α = γ = 90°, β = 114.022(2)°, V = 7636.4(6) Å^3, Z = 8, yellow prism 0.37 × 0.15 × 0.07 mm^3, μ = 3.896 mm^{-1}, min / max transmission = 0.36 / 0.72, T= 200(1) K, λ = 0.71073 Å, θ range = 1.23° to 3.58°, 84273 reflections measured, 11924 independent, R_{int} = 0.0514, completeness = 0.999, 460 parameters, 100 restraints, final R indices R1 [I>2σ(I)] = 0.0276 and wR2 (all data) = 0.0737, GOF on F^2 = 1.040, largest difference peak / hole = 1.26 / -0.83 e·Å^{-3}.

Crystal data for 3. $C_{41}H_{44}AuBF_4N_2O_4$, triclinic P -1, a = 8.2182(3) Å, b = 11.6914(4) Å, c = 21.1592(7) Å, α = 77.366(2)°, β = 79.609(2)°, γ = 87.410(2)°, V = 1951.23(12) Å^3, Z = 2, yellow prism 0.20 × 0.09 × 0.02 mm^3, μ = 7.607 mm^{-1}, min / max transmission = 0.27 / 0.93, T= 200(1) K, λ = 1.54178 Å, θ range = 3.88° to 66.67°, 28955 reflections measured, 6886 independent, R_{int} = 0.0298, completeness = 0.999, 588 parameters, 175 restraints, final R indices R1 [I>2σ(I)] = 0.0192 and wR2 (all data) = 0.0478, GOF on F^2 = 1.034, largest difference peak / hole = 0.53 / -0.55 e·Å^{-3}.

Crystal data for 5a. $C_{39.5}H_{44}AuBF_4N_2$, triclinic P -1, a = 6.8117(17) Å, b = 14.404(4) Å, c = 18.247(5) Å, α = 81.031(5)°, β = 86.785(4)°, γ = 87.919(5)°, V = 1764.9(8) Å^3, Z = 2, colorless block 0.12 × 0.21 × 0.26 mm^3, μ = 4.219 mm^{-1}, min / max transmission = 0.43 / 0.35, T= 200(1) K, λ = 0.71073 Å, θ range = 1.44° to 30.54°, 94607 reflections measured, 17922 independent, R_{int} = 0.0328, completeness = 0.995, 462 parameters, 50 restraints, final R indices R1 [I>2σ(I)] = 0.0380 and wR2 (all data) = 0.0815, GOF on F^2 = 1.074, largest difference peak / hole = 2.43 / -1.66 e·Å^{-3}.

Crystal data for 7. $C_{37.5}H_{33}AuBClF_4N_3$, monoclinic P $2_1/c$, a = 19.9010(5) Å, b = 10.4904(3) Å, c = 18.3807(5) Å, α = γ = 90°, β = 94.107(2)°, V = 3827.47(18) Å^3, Z = 4, colorless plate 0.38 × 0.19 × 0.02 mm^3, μ = 8.266 mm^{-1}, min / max transmission = 0.20 / 0.81, T= 200(1) K, λ = 1.54178 Å, θ range = 4.46° to 66.64°, 37141 reflections measured, 6769 independent, R_{int} = 0.0267, completeness = 0.999, 473 parameters, 63 restraints, final R indices R1 [I>2σ(I)] = 0.0235 and wR2 (all data) = 0.0633, GOF on F^2 = 1.020, largest difference peak / hole = 0.61 / -0.61 e·Å^{-3}.

Log $P_{o/w}$ determination by HPLC

Partition coefficients log P were determined by a reverse-phase HPLC polycratic method introduced by Minick et al.[28] The stationary phase was a Nucleosil C18 Htec 5 µm, 4.6 x 150 mm column (Macherey-Nagel). Mobile phase A was 20 mM MOPS, 0.15% decylamine (v/v) pH 7.4 in water saturated with 1-octanol and mobile phase B was 0.25% 1-octanol (v/v) in MeOH. In brief, solutions of compounds were prepared at 1 mM in MeOH. To 200 µL of those solutions,10 µL of uracil solution (5 mM in MeOH) were added in order to obtain a final concentration of 250 µM as unretained internal reference were repetitively injected in the column equilibrated with mobile phase B between 55 and 97 % at 1 ml/min. Retention times were measured on ChromNAV control center and the log k'w was determined by linear extrapolation of log k' at % B = 0. Log Po/w were calculated by using the following equation: Log $P_{o/w}$ = 0,31418 + 0,98452 log k'w.

Cell culture and cell growth inhibition

Human breast cancer cell lines MCF7 and MDA-MB-231 were cultivated in DMEM (Dulbecco's Modified Eagle Medium) containing GlutaMax I supplemented with 10% FBS and 1% kanamycin at 37 °C in a humidified atmosphere and 5% CO_2. Human ovarian cancer cells A2780 were cultured in RPMI1640 containing GlutaMax I supplemented with 10% FBS and 1% kanamycin at 37 °C in a humidified atmosphere and 5% CO_2. Non-cancerous cell line MCF10A was maintained in DMEM:F12 (1:1) cell culture media, 5 % heat inactivated horse serum, supplemented with HEPES (20 mM), L-glutamine (2 mM), epidermal growth factor (20 ng/mL), hydrocortisone (500 ng/mL), cholera toxin (100 ng/mL), and insulin (10 µg/mL). Cell viability was evaluated by using a colorimetric method based on the tetrazolium salt MTT [3-(4,5- dimethylthiazol-2-yl)-2,5-diphenyltetrazolium bromide], which is reduced by viable cells to yield purple formazan crystals. Cells were seeded in 96-well plates at a density of 40000 cells/mL (100 µL per well). After overnight attachment, a dilution series of the compounds were added in the medium, and cells were incubated for a further 72 h. Stock solutions of the complexes were prepared in water for cisplatin and the platinum and bimetallic compounds in DMSO. The percentage of DMSO in the culture medium did not exceed 1%. After 72 h, the medium was removed and the cells were incubated with MTT solution in PBS (10 µL of a 5 mg/mL) for 2-3 h of incubation. The formed purple formazan crystals were dissolved in 100 µL DMSO by thorough shaking, and the absorbance at 560 nm was read using a microplate reader (FLUOstar OPTIMA, BMG Labtech). Each test was performed with at least 3 replicates and repeated at least 3 times. The IC_{50} value is determined using GraphPad Prism 8.0 software.

BDE calculations

Calculations were performed using the Gaussian 09 software package.[43] Optimization of geometries, frequency and single point energy calculations were done using the PBW91 functional[44] with the following basis set: SDD[45–47] augmented with a set of f-orbital polarization functions[48] for Au and 6-31G(d,p) for others atoms.[49–51] The choice of the method was made following previous works reported on Au(III).[52] Definitions of the basis sets were obtained from the *Basis Set Exchange* library.[53–55] Bond dissociation energies were calculated from the electronic energy difference between the $[(C\hat{}C)Au]^+$ion + the (N^N) chelate and the $[(C\hat{}C)Au(N\hat{}N)]^+$ complex.

Low resolution mass spectrometry

Reaction with amino acids and guanine: Stock solutions of compounds **3** or **6a** (20 mM in DMSO) and each amino acid (100 mM in DMSO) were prepared separately. For the reactions with one amino acid

or guanine, a mixture of the solution of compounds **3** or **6a** with each amino acid or guanine was made: 250 µL of solution of **3** or **6a**, 50 µL of solution of amino acid or guanine and 200 µL of DMSO. For the reaction of **3** or **6a** with the mixture of all amino acids and guanine, the following mixture was made: 250 µL of solution of **3** or **6a** and 50 µL of solution of each amino acid and guanine. This leads to solution of 10 mM of **3** or **6a** with one equivalent of amino acid and guanine. Solutions were incubated at 37 °C for 24 h and were diluted to 100 µM with MeOH.

Reaction with glutathione: Two stock solutions were prepared. One of glutathione (GSH) at 200 mM in PBS (30.7 mg of GSH dissolved in 500 µL PBS) and one of the complex **3** or **6a** at 20 mM in DMSO (8.8 mg dissolved in 500 µL DMSO). Following this, five solutions, with respectively 0, 1, 2 and 5 equivalents of glutathione and a constant concentration of **3** or **6a** (10 mM) in a total volume of solution of 200 µL were prepared. After a 24-hour incubation at 37 ° C, the solutions were diluted 100 times in methanol for analysis by low resolution mass spectrometry.

Low resolution mass spectrometry experiments were performed using a modified Quattro II mass spectrometer (Micromass, Manchester, U.K.) equipped with an electrospray (ESI) source. The sample solutions were infused into the ESI source at a flow rate of ca. 400 $\mu L.h^{-1}$. The following source parameters were applied: in the positive ion mode: ESI capillary voltage 3.50 kV, cone voltage 30 V and in the negative ion mode: ESI capillary voltage -2.80 kV, cone voltage 30 V. Nitrogen was used as the desolvatation and nebulizing gas. The source and desolvatation temperatures were kept at 100 °C and 100 °C. The data were acquired and analyzed using Masslynx software (version 4.2).

High resolution mass spectrometry

HRMS spectra of $[(C^C)Au(N^N)]^+$ complexes were recorded on an Orbitrap mass spectrometer (see above). The HRMS experiments on association complexes of **3** or **6a** complexes with amino acids, guanine or glutathione were recorded on a Solarix XR FT-ICR mass spectrometer (Bruker Daltonics, Bremen, Germany) equipped with a 7T superconducting magnet and a dynamically harmonized ICR cell. Solutions of **3** or **6a** with cysteine, histidine and GSH were prepared at a 10 µM concentration in methanol by dilution of the corresponding mixture used in the low resolution mass spectrometry experiments (MeOH) and were infused into the electrospray ionization (ESI) source with a 180 µL/h flow rate. The following parameters were used for the ionization in the positive or in the negative mode: capillary voltage: 4.5 kV (positive mode), -3.5 kV (negative mode); drying gas flow rate: 3 L/ min; drying gas temperature: 200°C; nebulizer gas pressure: 1.8 bar. All analyses were recorded in 12 scans with a quadrupole accumulation time of 0.5 s and a transient length of 1.5 s. Identification of the adducts was achieved by comparison with theoretical masses of the adducts using the Bruker Compass Data Analysis software (5.0 SR1).

Uptake measurements

Cell samples preparation: Human ovarian adenocarcinoma cells (A2780) were grown in 25 cm^3 flasks in RPMI medium containing 10 % FBS for 24 h until confluence. Medium was discarded, the cells were rinsed with PBS and 5 mL of fresh medium containing or not 10 % FBS was added in each flask. Solutions of complexes **3**, **4**, **6a** and **6b** at 500 µM in DMSO were prepared and 50 µL of these solutions were added to the flasks to give a final concentration of 5 µM with 1 % DMSO. Cells were incubated with the compounds for 2 h at 37 °C, 5 % CO_2. Medium was then discarded, the cells washed with PBS and detached using a 0.05 % trypsin solution. Following quenching of trypsin with RPMI medium, the cells were isolated by centrifugation and the supernatant was discarded. The pellet was resuspended into 1 mL of PBS for AAS measurement and protein quantification.
Metal and protein quantification: For metal and protein quantification, the pellets were resuspended in demineralized water (1.0 mL) and lysed for 30 min by ultrasonication. The protein contents of lysates

were determined by the Bradford method, and the gold content was determined by a HRCS-AAS method described in a previous report.[38] The final result of the gold concentration was calculated from data obtained in two independent experiments and are expressed as nmol of gold per mg of cellular protein.

FRET assay

All work was performed on a QIAgen Rotor-Gene Q-Series PCR using the labelled oligonucleotides NRF2 (5'-FAM-d[GGG-AGC-GGG-ACG-GGG-GCC-GGG]-TAMRA-3'), NAST (5'-FAM-d[CCC-TCC-CGC-CCT-TGC-TCC-CTT-CCC]-TAMRA-3'), hTeloG (5'-FAM-d[$(GGG\text{-}TAA)_4$]-TAMRA-3'), DAP (5'-FAM-d[$(CCC\text{-}CCG)_4$-CCC-CC]-TAMRA-3'), and DS (5'-FAM-[TAT-AGC-TAT-A-HEG(18)-TAT-AGC-TAT-A]-TAMRA-3') (FAM = 6-carboxyfluorescein, TAMRA = 6-carboxytetramethyl-rhodamine). Strip-tubes were prepared containing a buffered solution (100 mM potassium chloride and 10 mM sodium cacodylate, pH 7.0) of 18 µL DNA and 2 µL ligand in DMSO with final concentrations of 0.2 µM and 1 µM for the DNA and ligand, respectively. Controls were performed using DMSO in place of the ligand solution. Samples were heated from 25 °C to 95 °C at increments of 1 °C, holding each temperature for 1 min. The fluorescence of each sample was measured using an excitation of 470 nm and the emission was detected at 510 nm. The melting temperatures (T_m) were calculated by taking the minima of the first derivative of each melting curve and reported as the average of three repeats with the associated errors as the standard deviations of the repeats.

TrxR inhibition assay

To determine the inhibition of mammalian thioredoxin reductase, a spectrophotometric assay was performed using commercially available rat liver TrxR (Sigma-Aldrich). The enzyme was diluted with distilled water to achieve a concentration of 2.5 U/mL. The gold complexes were freshly dissolved DMSO to get a stock solution of 10 mM. To a 25 µL aliquot of the enzyme solution, 25 µL of potassium phosphate buffer, pH 7.0, containing the complexes at different concentrations or solvent without compounds (control probe) was added, and the resulting solutions were incubated with moderate shaking for 75 min at 37 °C in a 96-well plate. Subsequently, to each well, 225 µL of reaction mixture (1 mL of reaction mixture consisted of 500 µL of potassium phosphate buffer, pH 7.0, 80 µL of EDTA solution (100 mM, pH 7.5), 20 µL of BSA solution (0.2%), 100 µL of NADPH solution (20 mM), and 300 µL of distilled water) was added. The reaction was started by the addition of 25 µL of an ethanolic solution of 5,5'-Dithiobis 2-nitrobenzoic acid (DTNB, 20 mM). After proper mixing, the formation of 5-TNB was monitored with a microplate reader (Perkin-Elmer Victor X4) at 405 nm in 10 s intervals for 10 min. The increase in 5-TNB concentration over time followed a linear trend ($R^2 \geq 0.99$), and the enzymatic activities were calculated as the slopes (increase in absorbance per second) thereof. For each tested compound, the noninterference with the assay components was confirmed by a negative control experiment using an enzyme free solution. The IC_{50} values were calculated as the concentration of complexes decreasing the enzymatic activity of the untreated control by 50% and are given as the means and standard deviations of 2 independent experiments.

Acknowledgments

The work was financially supported by Sorbonne Université and CNRS and was granted access to the HPC resources of the HPCaVe Centre at UPMC-Sorbonne Université. B.B. thanks Dr. Cédric Przybylski for HR-MS analyses. B.B. thanks Dr. Patricia Forgez for providing A2780 and MCF-10A cells. Financial support from the National FT-ICR network (FR 3624 CNRS) for conducting the research is gratefully

acknowledged. P.S. was supported by the BBSRC Norwich Research Park Biosciences Doctoral Training Partnership (grant number BB/M011216/1).

Abbreviations used

NHC, nucleophic heterocyclic carbene; DMSO, dimethylsulfoxide; PBS, phosphate buffer saline; GSH, glutathione; TrxR, thioredoxin reductase

References

[1] I. Ott, *Coord. Chem. Rev.* **2009**, *253*, 1670–1681.
[2] B. Bertrand, A. Casini, *Dalton Trans* **2014**, *43*, 4209–4219.
[3] T. Zou, C. T. Lum, C.-N. Lok, J.-J. Zhang, C.-M. Che, *Chem. Soc. Rev.* **2015**, *44*, 8786–8801.
[4] D. Wang, S. J. Lippard, *Nat. Rev. Drug Discov.* **2005**, *4*, 307–320.
[5] B. Bertrand, M. R. M. Williams, M. Bochmann, *Chem. – Eur. J.* **2018**, *24*, 11840–11851.
[6] L. Messori, F. Abbate, G. Marcon, P. Orioli, M. Fontani, E. Mini, T. Mazzei, S. Carotti, T. O'Connell, P. Zanello, *J. Med. Chem.* **2000**, *43*, 3541–3548.
[7] S. Gukathasan, S. Parkin, S. G. Awuah, *Inorg. Chem.* **2019**, *58*, 9326–9340.
[8] C. Y.-S. Chung, S.-K. Fung, K.-C. Tong, P.-K. Wan, C.-N. Lok, Y. Huang, T. Chen, C.-M. Che, *Chem. Sci.* **2017**, *8*, 1942–1953.
[9] M. Negom Kouodom, L. Ronconi, M. Celegato, C. Nardon, L. Marchiò, Q. P. Dou, D. Aldinucci, F. Formaggio, D. Fregona, *J. Med. Chem.* **2012**, *55*, 2212–2226.
[10] R. T. Mertens, S. Parkin, S. G. Awuah, *Chem. Sci.* **2020**, *11*, 10465–10482.
[11] J.-J. Zhang, R. W.-Y. Sun, C.-M. Che, *Chem. Commun.* **2012**, *48*, 3388.
[12] B. Bertrand, S. Spreckelmeyer, E. Bodio, F. Cocco, M. Picquet, P. Richard, P. Le Gendre, C. Orvig, M. A. Cinellu, A. Casini, *Dalton Trans.* **2015**, *44*, 11911–11918.
[13] S. Carboni, A. Zucca, S. Stoccoro, L. Maiore, M. Arca, F. Ortu, C. Artner, B. K. Keppler, S. M. Meier-Menches, A. Casini, M. A. Cinellu, *Inorg. Chem.* **2018**, *57*, 14852–14865.
[14] R. W.-Y. Sun, C.-N. Lok, T. T.-H. Fong, C. K.-L. Li, Z. F. Yang, T. Zou, A. F.-M. Siu, C.-M. Che, *Chem. Sci.* **2013**, *4*, 1979.
[15] B. Bertrand, J. Fernandez-Cestau, J. Angulo, M. M. D. Cominetti, Z. A. E. Waller, M. Searcey, M. A. O'Connell, M. Bochmann, *Inorg. Chem.* **2017**, *56*, 5728–5740.
[16] X.-Q. Zhou, I. Carbo-Bague, M. A. Siegler, J. Hilgendorf, U. Basu, I. Ott, R. Liu, L. Zhang, V. Ramu, A. P. IJzerman, S. Bonnet, *JACS Au* **2021**, *1*, 380–395.
[17] J. J. Yan, A. L.-F. Chow, C.-H. Leung, R. W.-Y. Sun, D.-L. Ma, C.-M. Che, *Chem. Commun.* **2010**, *46*, 3893.
[18] S. Jürgens, V. Scalcon, N. Estrada-Ortiz, A. Folda, F. Tonolo, C. Jandl, D. L. Browne, M. P. Rigobello, F. E. Kühn, A. Casini, *Bioorg. Med. Chem.* **2017**, *25*, 5452–5460.
[19] M. Williams, A. I. Green, J. Fernandez-Cestau, D. L. Hughes, M. A. O'Connell, M. Searcey, B. Bertrand, M. Bochmann, *Dalton Trans* **2017**, *46*, 13397–13408.
[20] R. Usón, J. Vincente, J. A. Cirac, M.-T. Chicote, **1980**, *198*, 105–112.
[21] B. David, U. Monkowius, J. Rust, C. W. Lehmann, L. Hyzak, F. Mohr, *Dalton Trans* **2014**, *43*, 11059–11066.
[22] K. T. Chan, G. S. M. Tong, Q. Wan, G. Cheng, C. Yang, C.-M. Che, *Chem. - Asian J.* **2017**, *12*, 2104–2120.
[23] L. Rocchigiani, J. Fernandez-Cestau, G. Agonigi, I. Chambrier, P. H. M. Budzelaar, M. Bochmann, *Angew. Chem. Int. Ed.* **2017**, *56*, 13861–13865.

[24] I. Chambrier, L. Rocchigiani, D. L. Hughes, P. M. H. Budzelaar, M. Bochmann, *Chem. - Eur. J.* **2018**, *24*, 11467–11474.
[25] V. K.-M. Au, K. M.-C. Wong, N. Zhu, V. W.-W. Yam, *J. Am. Chem. Soc.* **2009**, *131*, 9076–9085.
[26] J. Fernandez-Cestau, B. Bertrand, M. Blaya, G. A. Jones, T. J. Penfold, M. Bochmann, *Chem. Commun.* **2015**, *51*, 16629–16632.
[27] C. A. Lipinski, F. Lombardo, B. W. Dominy, P. J. Feeney, *Adv. Drug Deliv. Rev.* **2001**, *46*, 3–26.
[28] D. J. Minick, J. H. Frenz, M. A. Patrick, D. A. Brent, *J. Med. Chem.* **1988**, *31*, 1923–1933.
[29] H. Yao, G. He, S. Yan, C. Chen, L. Song, T. J. Rosol, X. Deng, *Oncotarget* **2017**, *8*, 1913–1924.
[30] B. Bertrand, C. Botuha, J. Forté, H. Dossmann, M. Salmain, *Chem. – Eur. J.* **2020**, *26*, 12846–12861.
[31] M. Coronnello, E. Mini, B. Caciagli, M. A. Cinellu, A. Bindoli, C. Gabbiani, L. Messori, *J. Med. Chem.* **2005**, *48*, 6761–6765.
[32] N. Traverso, R. Ricciarelli, M. Nitti, B. Marengo, A. L. Furfaro, M. A. Pronzato, U. M. Marinari, C. Domenicotti, *Oxid. Med. Cell. Longev.* **2013**, *2013*, 972913.
[33] H. H. W. Chen, M. T. Kuo, *Met.-Based Drugs* **2010**, *2010*, 1–7.
[34] A. Casini, M. A. Cinellu, G. Minghetti, C. Gabbiani, M. Coronnello, E. Mini, L. Messori, *J. Med. Chem.* **2006**, *49*, 5524–5531.
[35] M. R. M. Williams, B. Bertrand, D. L. Hughes, Z. A. E. Waller, C. Schmidt, I. Ott, M. O'Connell, M. Searcey, M. Bochmann, *Metallomics* **2018**, *10*, 1655–1666.
[36] J.-J. Zhang, R. W.-Y. Sun, C.-M. Che, *Chem. Commun.* **2012**, *48*, 3388.
[37] S. Spreckelmeyer, C. Orvig, A. Casini, *Molecules* **2014**, *19*, 15584–15610.
[38] C. Schmidt, B. Karge, R. Misgeld, A. Prokop, R. Franke, M. Brönstrup, I. Ott, *Chem. - Eur. J.* **2017**, *23*, 1869–1880.
[39] C. K.-L. Li, R. W.-Y. Sun, S. C.-F. Kui, N. Zhu, C.-M. Che, *Chem. - Eur. J.* **2006**, *12*, 5253–5266.
[40] P. Gratteri, L. Massai, E. Michelucci, R. Rigo, L. Messori, M. A. Cinellu, C. Musetti, C. Sissi, C. Bazzicalupi, *Dalton Trans.* **2015**, *44*, 3633–3639.
[41] A. Bindoli, M. P. Rigobello, G. Scutari, C. Gabbiani, A. Casini, L. Messori, *Coord. Chem. Rev.* **2009**, *253*, 1692–1707.
[42] M. Elie, F. Sguerra, F. Di Meo, M. D. Weber, R. Marion, A. Grimault, J.-F. Lohier, A. Stallivieri, A. Brosseau, R. B. Pansu, J.-L. Renaud, M. Linares, M. Hamel, R. D. Costa, S. Gaillard, *ACS Appl. Mater. Interfaces* **2016**, *8*, 14678–14691.
[43] M. J. Frisch, G. W. Trucks, H. B. Schlegel, G. E. Scuseria, M. A. Robb, J. R. Cheeseman, G. Scalmani, V. Baronne, B. Mennucci, G. A. Petersson, H. Nakatsuji, M. Caricato, X. Li, H. P. Hratchian, A. F. Izmaylov, J. Bloino, G. Zheng, J. L. Sonnenberg, M. Hada, M. Ehara, K. Toyota, R. Fukuda, J. Hasegawa, M. Ishida, T. Nakajima, Y. Honda, O. Kitao, H. Nakai, T. Vreven, J. A. Montgomery, Jr., J. E. Peralta, F. Ogliaro, M. Bearpark, J. J. Heyd, E. Brothers, K. N. Kudin, V. N. Staroverov, R. Kobayashi, J. Normand, K. Raghavachari, A. Rendell, J. C. Burant, S. S. Iyengar, J. Tomasi, M. Cossi, N. Rega, J. M. Millam, M. Klene, J. E. Knox, J. B. Cross, V. Bakken, C. Adamo, J. Jaramillo, R. Gomperts, R. E. Stratmann, O. Yazyev, A. J. Austin, R. Cammi, C. Pomelli, J. W. Ochterski, R. L. Martin, K. Morokuma, V. G. Zakrzewski, G. H. Voth, P. Salvador, J. J. Dannenberg, S. Dapprich, A. D. Daniels, Ö. Farkas, J. B. Foresman, J. V. Ortiz, J. Cioslowski, D. J. Fox, *Gaussian 09, Revision D.01*, Gaussian, Inc., Wallingford CT, **2009**.
[44] J. P. Perdew, K. Burke, Y. Wang, *Phys. Rev. B* **1996**, *54*, 16533–16539.

[45] D. Andrae, U. Häußermann, M. Dolg, H. Stoll, H. Preuß, *Theor. Chim. Acta* **1990**, *77*, 123–141.
[46] T. H. Dunning Jr., P. J. Hay, in *Methods Electron. Struct. Theory*, Plenum, New York, **1977**, pp. 1–28.
[47] U. Wedig, M. Dolg, H. Stoll, H. Preuß, in *Quantum Chem. Chall. Transit. Met. Coord. Chem.*, **1986**, p. 79.
[48] A. W. Ehlers, M. Böhme, S. Dapprich, A. Gobbi, A. Höllwarth, V. Jonas, K. F. Köhler, R. Stegmann, A. Veldkamp, G. Frenking, *Chem. Phys. Lett.* **1993**, *208*, 111–114.
[49] W. J. Hehre, R. Ditchfield, J. A. Pople, *J. Chem. Phys.* **1972**, *56*, 2257–2261.
[50] P. C. Hariharan, J. A. Pople, *Theor. Chim. Acta* **1973**, *28*, 213–222.
[51] T. Clark, J. Chandrasekhar, G. W. Spitznagel, P. V. R. Schleyer, *J. Comput. Chem.* **1983**, *4*, 294–301.
[52] J. Rodriguez, G. Szalóki, E. D. S. Carrizo, N. Saffon-Merceron, K. Miqueu, D. Bourissou, *Angew. Chem. Int. Ed.* **2020**, *59*, 1511–1515.
[53] D. Feller, *J. Comput. Chem.* **1996**, *17*, 1571–1586.
[54] K. L. Schuchardt, B. T. Didier, T. Elsethagen, L. Sun, V. Gurumoorthi, J. Chase, J. Li, T. L. Windus, *J. Chem. Inf. Model.* **2007**, *47*, 1045–1052.
[55] B. P. Pritchard, D. Altarawy, B. Didier, T. D. Gibson, T. L. Windus, *J. Chem. Inf. Model.* **2019**, *59*, 4814–4820.

Table of content

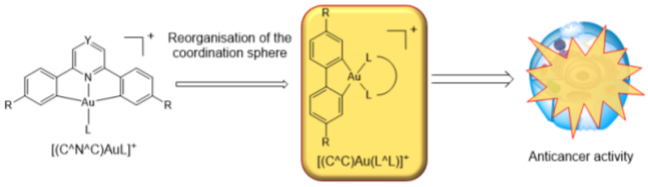

The reorganisation of the coordination sphere of the $[(C^N^C)AuL]^+$ scaffold led to the establishment of $[(C^C)Au(N^N)]^+$ family with a preserved redox stability but an enhanced reactivity toward biomolecules making it a new class of organogold anticancer agent.